Supplement of Earth Surf. Dynam., 13, 1157–1179, 2025 https://doi.org/10.5194/esurf-13-1157-2025-supplement © Author(s) 2025. CC BY 4.0 License.





Supplement of

Progressive destabilization of a freestanding rock pillar in permafrost on the Matterhorn (Swiss Alps): Hydro-mechanical modeling and analysis

Samuel Weber et al.

Correspondence to: Samuel Weber (samuel.weber@slf.ch)

The copyright of individual parts of the supplement might differ from the article licence.

This supporting material provides additional data and analyses that complement the main study on the progressive destabilization of a freestanding rock pillar in permafrost at the Matterhorn (CH). It includes supplementary figures illustrating rock instability evolution, such as dip angle changes from point cloud analysis and monthly/yearly aggregated inclination measurements. Additionally, it examines the potential influence of cohesion on the laboratory-inferred friction angle. The document also presents unrelated kinematic measurements, including fracture displacement observations, as well as extended environmental forcing data, such as snow height measurements, borehole temperature time series from the Hörnli hut, and periods with non-conductive heat fluxes have been identified. Together, these data provide a broader context for understanding the complex interactions between thermal, mechanical, and kinematic processes governing rock slope stability in mountain permafrost regions.

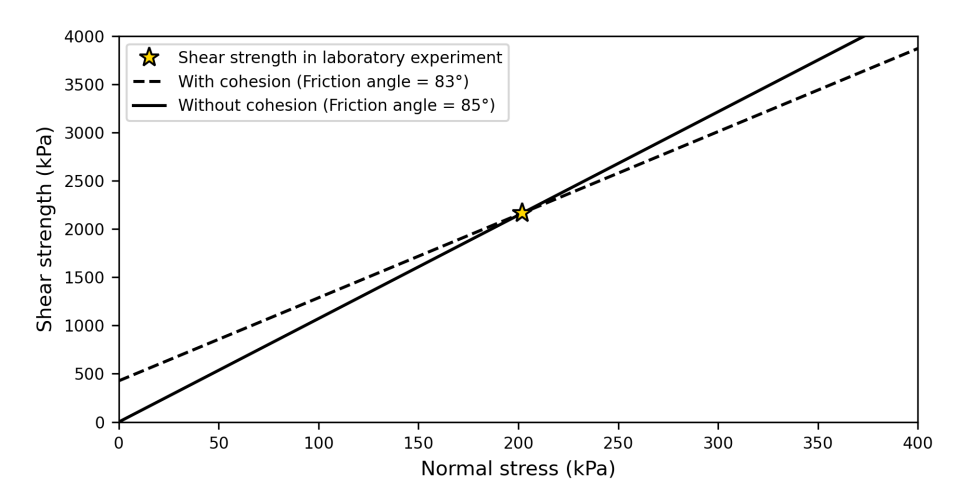


Figure S1. Influence of cohesion according to the Mohr-Coulomb criterion for ice-filled fractures (Mamot et al., 2018) on the laboratory-inferred friction angle.

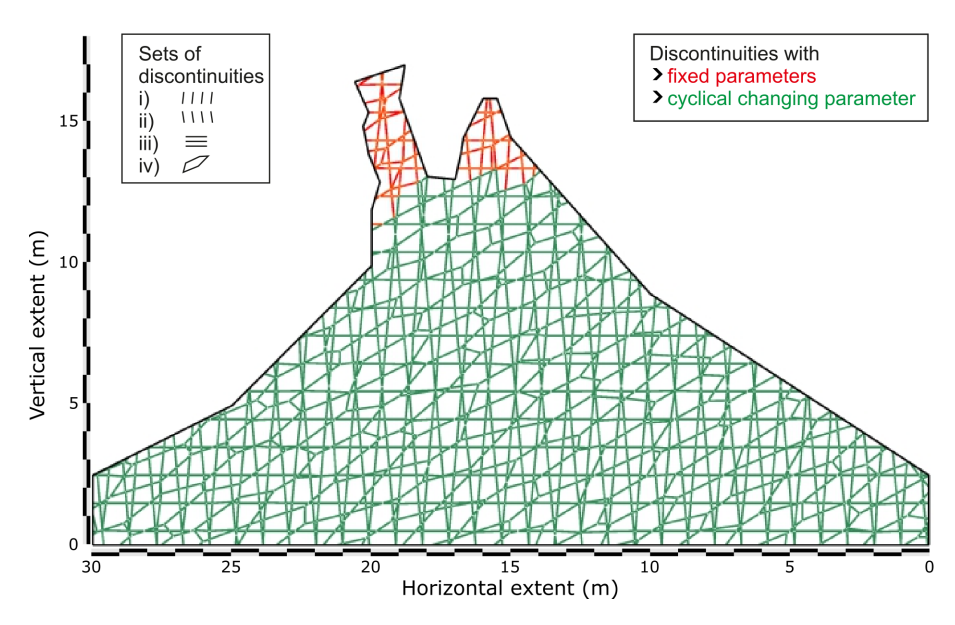


Figure S2. Topography and internal structure of the UDEC model indicated by four different sets of discontinuities. Discontinuities in the upper part of the pillar and ridge (red color) were assigned fixed shear parameters throughout all simulations: $\phi = 80^{\circ}$, c=1 MPa, and $\sigma_{tensile}$ =0.5 MPa, while those in the bedrock below (green color) were assigned alternating friction angles, $\phi = 80^{\circ}$ or 40° , accounting for the cyclical changes (c = 0 MPa, and $\sigma_{tensile} = 0$ MPa).

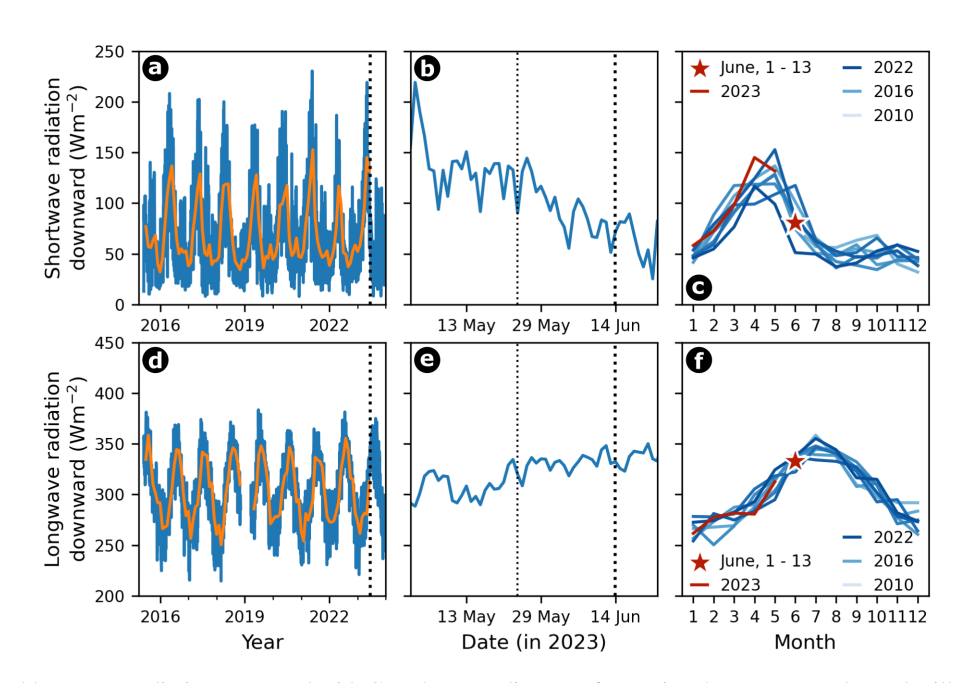


Figure S3. Short- and longwave radiation measured with CNR4 Net Radiometer from Kipp & Zonen near the rock pillar at 3500 m asl.

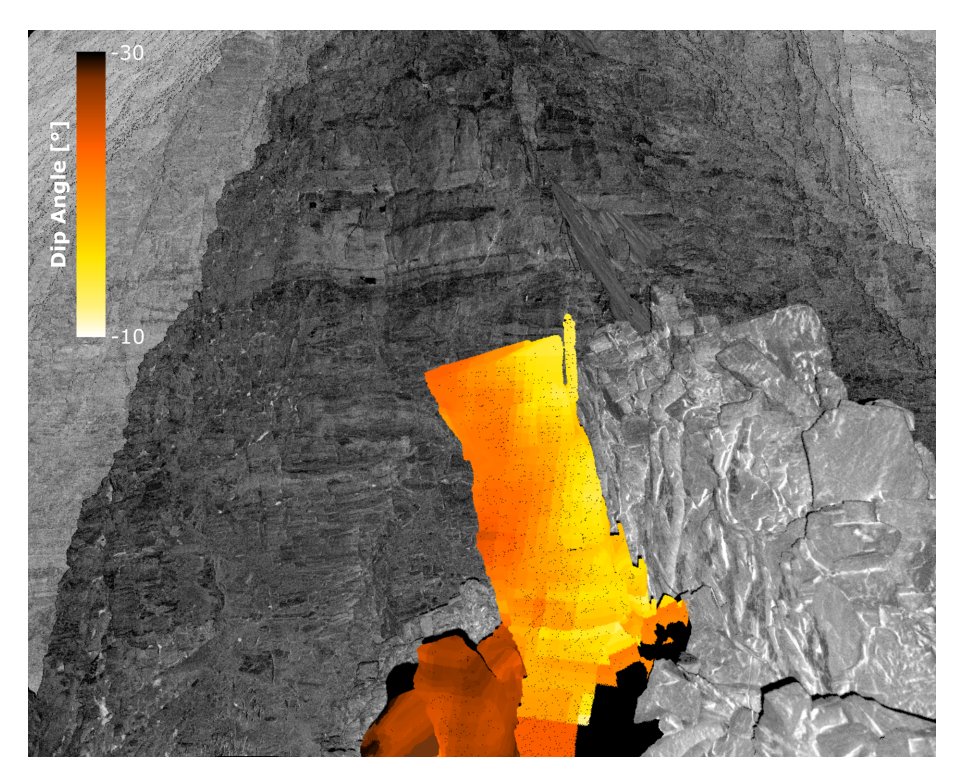


Figure S4. Point cloud analysis showing the dip angle (rotation) between the laser scans on 27 July 2015 and 20 August 2018.

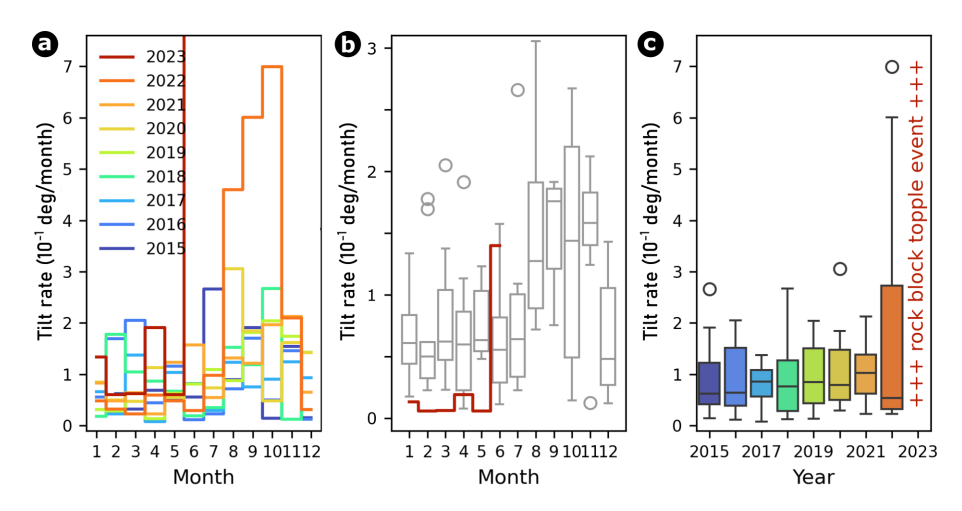


Figure S5. Monthly and annual rotational displacement rates (tilt rate) derived from an in-situ inclinometer mounted on the rock pillar.

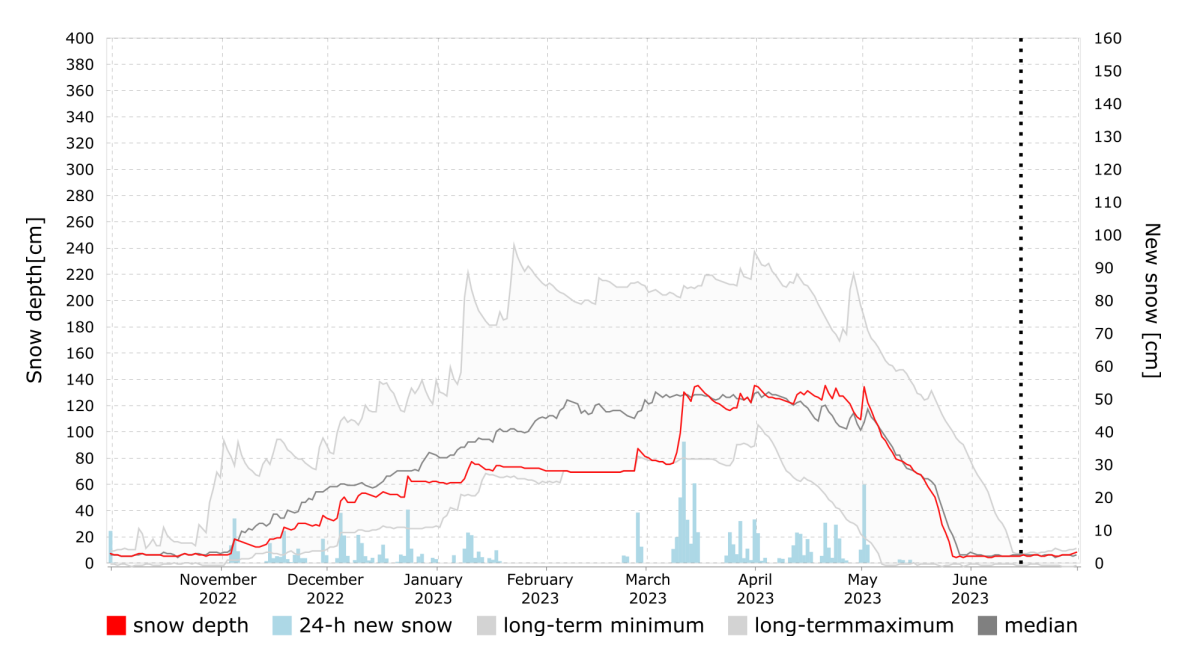


Figure S6. IMIS snow station Stafelalp/ZER4 at 2408 m asl showing winter 2022-2023 in a 16-year comparison (Data source: Intercantonal Measurement and Information System IMIS, 2023). At the study site located 1000 m higher, the later-occurring enhanced snowmelt likely played a role in the events leading up to the collapse of the rock pillar on 13 June (indicated by the dashed black line).

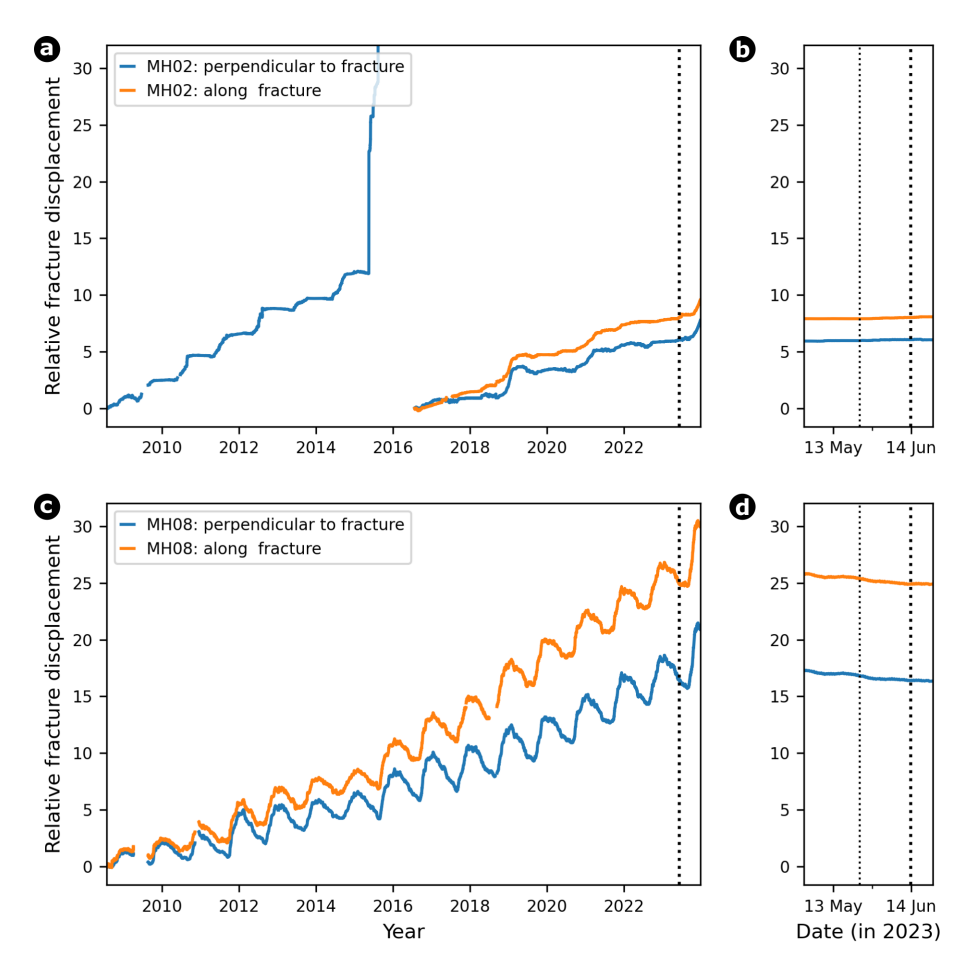


Figure S7. Fracture displacement time series for crackmeters at position MH02 and MH08 for the (a+c) period 2008-2023 and (b+d) zoom into the period from 1 May to 23 June 2023 with dotted and dashed black lines indicating the estimated onset of water infiltration and the time of collapse of the rock pillar, respectively (for sensor and instrumentation details, see Weber et al., 2019). Neither crackmeter shows an anomaly in the fracture displacement patterns coincident to the collapse of the freestanding rock pillar.

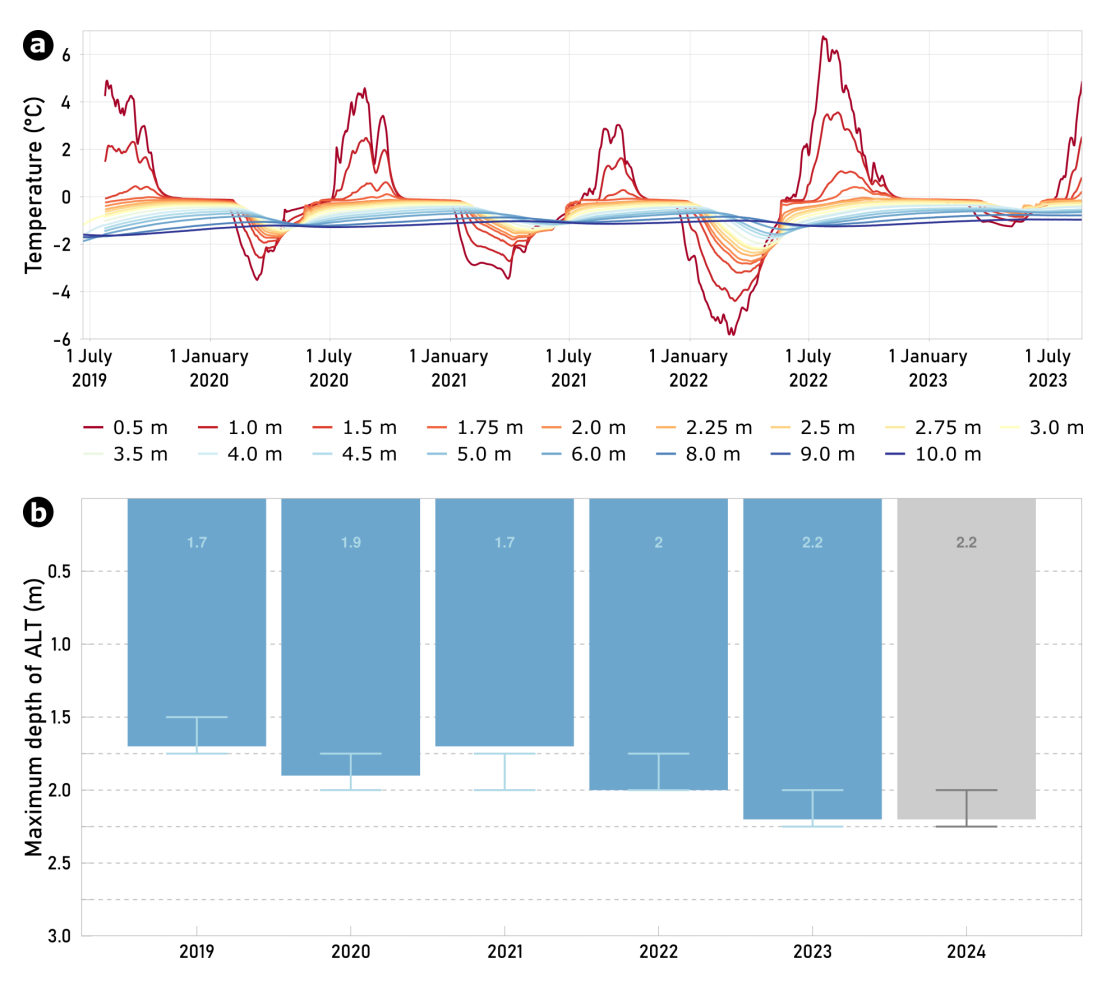


Figure S8. (a) Borehole temperature time series and (b) maximum depth of ALT (active layer thickness) depth measured next to the Hörnli hut (Data source: SLF Davos).

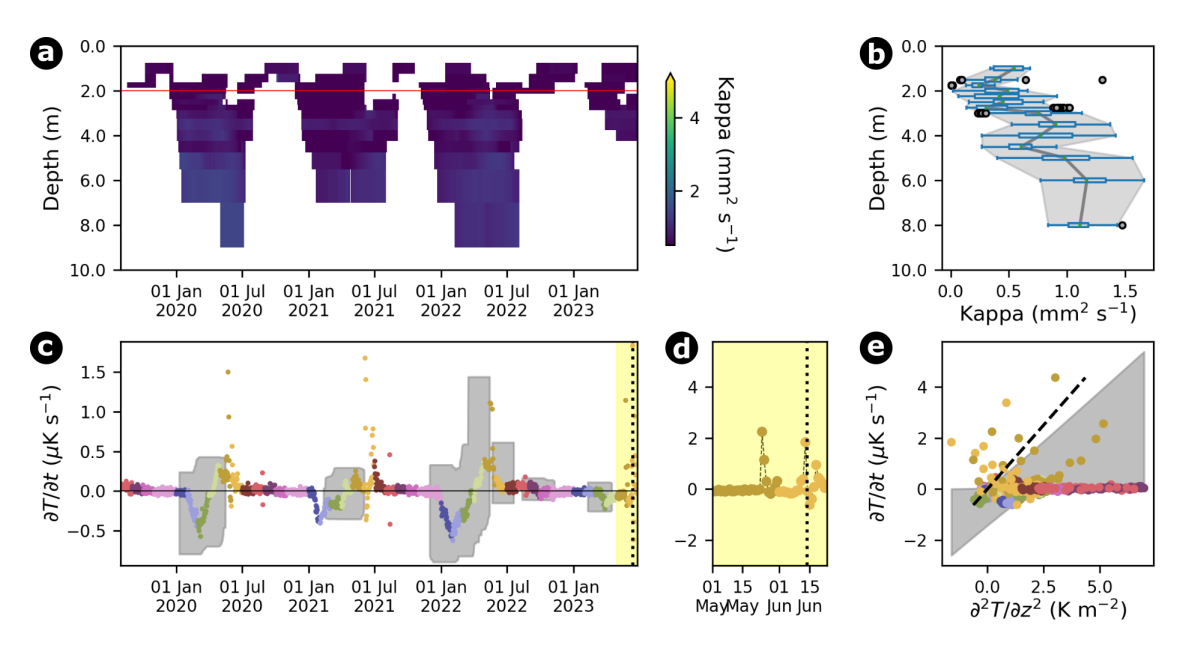


Figure S9. Thermal diffusivity values, derived through linear regression analysis of the heat conduction equation for the SLF borehole Hörnli hut MAT_0311 (following Weber and Cicoira, 2024). For the top 10 m, (a) shows the time-depths-thermal diffusivity plot and (b) a profile with boxplots of all diffusivity values for each depth instrumented with a thermistor. (c) The temperature rate at 2 m depth for the entire time series (yellow area is a zoom from 1 May to 23 June 2023 is shown in (d) with different y-scale; vertical dashed line indicates time of failure) and (e) a temperature-rate/temperature-Laplacian scatter combining observations (colored by month) and the 95% prediction bands of all valid linear regression models (a gray area with large scattering due to seasonal evolution) that can be used to identify outliers and, thus, the occurrence of non-conductive processes.

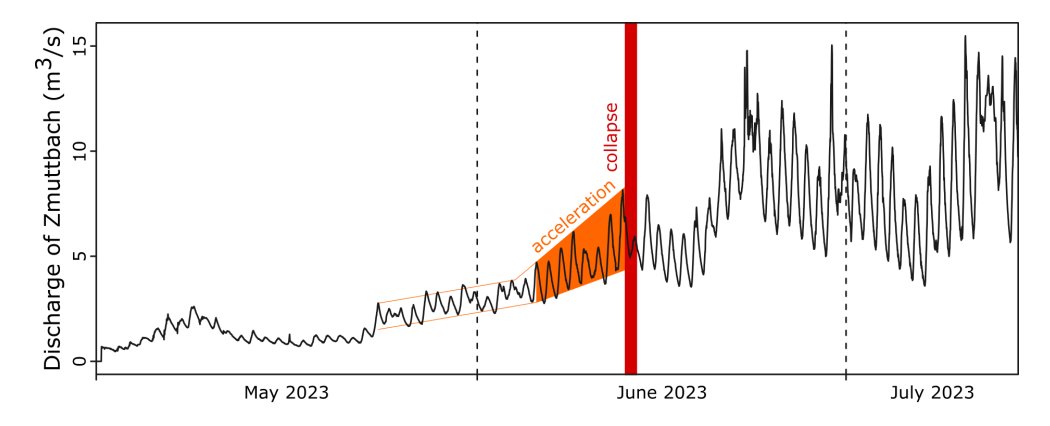


Figure S10. Discharge time series (black) measured at Zmuttbach above Zermatt at approx. 2000 m asl (Data source: ALPIQ Hydropower). Vertical dashed lines indicate the beginning of a new month. Red bar indicates the day of the Matterhorn rock pillar collapse on 13 June 2023. While the orange lines qualitatively indicate the band of daily fluctuations in measures discharge, the orange area refers to the measured acceleration phase of the rock pillar prior to failure.

10 References

- Intercantonal Measurement and Information System IMIS: IMIS measuring network, https://doi.org/10.16904/envidat.406, 2023.
- Mamot, P., Weber, S., Schröder, T., and Krautblatter, M.: A temperature- and stress-controlled failure criterion for ice-filled permafrost rock joints, The Cryosphere, 12, 3333–3353, https://doi.org/10.5194/tc-12-3333-2018, 2018.
- Weber, S. and Cicoira, A.: Thermal diffusivity of permafrost in the Swiss Alps determined from borehole temperature data, EGUsphere, pp. 1–24, https://doi.org/10.5194/egusphere-2024-2652, 2024.
 - Weber, S., Beutel, J., Da Forno, R., Geiger, A., Gruber, S., Gsell, T., Hasler, A., Keller, M., Lim, R., Limpach, P., Meyer, M., Talzi, I., Thiele, L., Tschudin, C., Vieli, A., Vonder Mühll, D., and Yücel, M.: A decade of detailed observations (2008–2018) in steep bedrock permafrost at the Matterhorn Hörnligrat (Zermatt, CH), Earth System Science Data, 11, 1203–1237, https://doi.org/10.5194/essd-11-1203-2019, 2019.